Nature of intrinsic and extrinsic electron trapping in SiO_2

Al-Moatasem El-Sayed,[1,*] Matthew B. Watkins,[1,†] Valery V. Afanas'ev,[2,‡] and Alexander L. Shluger[1,§]
[1]*Department of Physics and Astronomy and London Centre for Nanotechnology, University College London, Gower Street, London, WC1E 6BT, United Kingdom*
[2]*Department of Physics, University of Leuven, Celestijnenlaan 200D, 3001 Leuven, Belgium*

(Received 2 August 2013; published 10 March 2014)

Using classical and *ab initio* calculations we demonstrate that extra electrons can be trapped in pure crystalline and amorphous SiO_2 (a-SiO_2) in deep band gap states. The structure of trapped electron sites in pure a-SiO_2 is similar to that of Ge electron centers and so-called $[SiO_4/Li]^0$ centers in α quartz. Classical potentials were used to generate amorphous silica models and density functional theory to characterize the geometrical and electronic structures of trapped electrons in crystalline and amorphous silica. The calculations demonstrate that an extra electron can be trapped at a Ge impurity in α quartz in six different configurations. An electron in the $[SiO_4/Li]^0$ center is trapped on a regular Si ion with the Li ion residing nearby. Extra electrons can trap spontaneously on pre-existing structural precursors in amorphous SiO_2, while the electron self-trapping in α quartz requires overcoming a barrier of about 0.6 eV. The precursors for electron trapping in amorphous SiO_2 comprise wide ($\geqslant 132^\circ$) O–Si–O angles and elongated Si–O bonds at the tails of corresponding distributions. Using this criterion, we estimate the concentration of these electron trapping sites at $\approx 4 \times 10^{19}$ cm^{-3}.

DOI: 10.1103/PhysRevB.89.125201 PACS number(s): 71.23.An, 71.55.Jv, 72.15.Rn

I. INTRODUCTION

The mechanisms of electron and hole trapping in SiO_2 and the nature of trapping sites are important for our understanding of a wide range of physical phenomena, such as radiation-induced damage and electrical breakdown, and for applications in fiber optics and microelectronics. In particular, electron trapping is known to have a dramatic effect on the performance and reliability of electronic devices employing SiO_2 as gate insulator and charge trap flash memory devices [1,2]. Hole trapping in silica has been relatively well understood, with models of trapped holes [3–6] and several hole trapping defects well established [7–9]. However, identifying sites responsible for electron trapping in silica, bulk, and surface, has proved particularly challenging. This is because of a large number of possible charge redistribution channels and the presence of water and impurities in most samples. So far, the dominant electron traps have been associated with impurity-related centers, in particular, the hydrogen-related network fragments [10–13]. It has been well established that electrons can be trapped by Ge impurities substituting for Si in both α quartz [14] and in a-SiO_2 [15], with models of these centers recently revisited by Griscom [16]. A defect consisting of an extra electron trapped at a four-coordinated silicon atom and stabilized by an adjacent interstitial Li ion has been observed in α quartz [17].

However, little is still known regarding the possibility of *intrinsic* electron trapping in the a-SiO_2 network. Bersuker *et al.* used molecular models to suggest that electrons can be trapped by Si–O bonds in a-SiO_2, leading to their weakening and thus facilitating Si–O bond dissociation [18]. Using a F_3Si–O–SiF_3 cluster, chosen to simulate the structure of two SiO_4 tetrahedra, they showed that an extra electron introduced into this cluster may localize on a Si–O bond, causing the other Si–O bond associated with the oxygen to contract. The extra electron localizes in an oxygen p state, significantly weakening one Si–O bond. The O–Si–O angle after the electron has been localized on the Si–O bond is 144° in this cluster model. Further calculations by Camellone *et al.* have shown that electrons can be trapped in a nondefective continuum random network model of a-SiO_2 [19]. In this study, several structures of 72 atoms of a-SiO_2 were generated using classical molecular dynamics (MD) simulations. The electronic structures of these models were then calculated using density functional theory, utilizing the generalized gradient approximation (GGA) and also including the self-interaction correction. The potential energy surface of the system with an extra electron was explored along a reaction coordinate defined as the elongation of one Si–O bond. The global energy minimum corresponds to the neutral equilibrium geometry where the electron is delocalized over the system, but a metastable state was found where the Si–O bond was extended to 1.83 Å. In this state, an electron is localized on the Si atom. Extension of the Si–O bond and electron localization also resulted in expansion of the O–Si–O angle up to 156.44°. The barrier from the delocalized state to the metastable localized state was found to be 0.23 eV, with the localized state higher in energy by 0.17 eV. Recent calculations have also demonstrated that silicon dangling bonds at SiO_2 surfaces are deep electron traps and can form the corresponding negatively charged defects [20]. However, these theoretical predictions have not yet been confirmed experimentally due to challenges in identifying defect centers.

Unlike in optical fibers and other optical devices, where electrons and holes are created by electronic excitation, in metal-oxide-semiconductor (MOS) devices they are often injected from Si substrate. For example, electron trapping at an energy of 2.8 eV below the conduction band of a-SiO_2 has been observed using photon-stimulated tunneling experiments in device-grade oxides grown on Si and SiC crystals in a series of papers [21–24]. Further low-temperature capacitance [25]

*al-moatasem.el-sayed.10@ucl.ac.uk
†matthew.watkins@ucl.ac.uk
‡valeri.afanasiev@fys.kuleuven.be
§a.shluger@ucl.ac.uk

 ©2014 American Physical Society

and Hall effect measurements [26,27] on 4H-SiC MOS devices revealed that the density of these electron trapping states can be as high as 10^{14} cm^{-2} eV^{-1}. The trap density of 10^{13} cm^{-2} measured inside a 2-nm thick near-interface SiO_2 layer [21,24] corresponds to $\approx 5 \times 10^{19}$ cm^{-3} in terms of volume concentration. This is much higher than observed densities of the established intrinsic defects in thermally grown a-SiO_2. The absence of a comparable density of electron traps in bulk a-SiO_2 and the strong sensitivity of electron trapping to the incorporation of nitrogen at the interface [28,29] suggests that electron trapping at 2.8 eV deep centers takes place not on pre-existing defects but rather in the oxide network itself. Whether the substrate plays any role in stabilizing these traps remains unclear. These results, as well as the previous theoretical calculations described above, motivate further investigation into the possibility of electron trapping in amorphous silica network.

In this paper we show that electrons can be trapped in a continuous nondefective a-SiO_2 network forming deep electron states in the gap. The geometric structure of these centers is similar to that of electrons trapped by Ge impurities in a-SiO_2 [30], where the key to the electron trapping is the wide opening of the O–Ge–O angle, or Li centers in quartz, where it is facilitated by the opening of the O–Si–O angle. It turns out that precursor Si sites with wide enough O–Si–O angles naturally present in a-SiO_2 structure can facilitate spontaneous electron trapping at these sites. Using this *fingerprint* we estimate the concentration of intrinsic electron trapping sites in a-SiO_2. The preliminary results of this work have been published in Ref. [31].

II. DETAILS OF CALCULATIONS

A. Classical calculations

The calculations presented in this work make use of both classical force fields and *ab initio* theory. The ReaxFF [32] force field was used to generate 20 models of amorphous SiO_2, each containing 216 atoms, modeled within periodic boundary conditions. ReaxFF was parametrized to reproduce the properties of various silica polymorphs, small silica clusters, and silicon polymorphs [33]. This force field allows one to calculate Si and O atoms in varying oxidation states based on the instantaneous geometry of the system, which is particularly important for modeling Si/SiO_2 interfaces. This is accomplished by assigning a charge-dependent atomic energy and exploiting the electronegativity equalization principle [34]. We used this force field in this work with a view to studying the effect of the Si and SiC substrates in future studies.

The extended bulk silica structures used in this study—containing up to 401 760 atoms—were generated using the BKS potential [35]. This Buckingham-type potential allows one to perform calculations much faster than the ReaxFF potential and is more suited to creating large a-SiO_2 structures. As we show below, comparing results obtained with two very different force fields gives more confidence in our predictions. All classical atomistic simulations were performed using the LAMMPS code [36].

To generate amorphous structures, classical molecular dynamics simulations were run using ReaxFF or BKS to melt and quench crystalline SiO_2 structures into an amorphous state in a manner similar to previously reported calculations [37–39]. Starting from supercells with a β-cristobalite structure, the system was equilibrated at 300 K and pressure of 1 atm. Maintaining the pressure at 1 atm, the temperature was linearly ramped to 5000 K (in the ReaxFF simulations) or 7000 K (in the BKS simulations). The temperature was maintained at 5000 K/7000 K for 40 ps and then brought down to 0 K at a rate of 8 K/ps. The resulting structures were then characterized by calculating basic geometrical properties, such as bond length and bond angle distributions, density, and total structure factors. The 20 models generated using ReaxFF contain no coordination defects, i.e., all Si atoms are bonded to four O atoms and all O atoms are bonded to two Si atoms. The calculated Si–O bond lengths of the ReaxFF structures average at 1.58 Å, while the O–Si–O angles average at 109° and the Si–O–Si angles average at 155°. Densities of the ReaxFF a-SiO_2 structures ranged from 2.05 to 2.20 g cm^{-3}, averaging at 2.13 g cm^{-3}. Total structure factors were also calculated and showed three sharp peaks at 1.58 Å, 2.54 Å, and 3.09 Å. These geometrical parameters indicate that the bond lengths are underestimated with ReaxFF, while the Si–O–Si bond angles are slightly overestimated. The BKS structures have a higher density of 2.37 g cm^{-3}. The Si–O bond lengths of the BKS structures averaged at 1.61 Å, while the O–Si–O angles average at 108° and the Si–O–Si angles average at 142 °.

B. Density functional theory calculations

Density functional theory (DFT), implemented in the CP2K code, was used to further optimize geometries of the ReaxFF structures and calculate their electronic structures [40]. The nonlocal functional PBE0_TC_LRC was used in all calculations with a cutoff radius of 2.0 Å [41]. The functional form of the PBE0_TC_LRC is very similar to the Heyd, Scuseria, and Ernzerhof (HSE) functional [42] and, in our experience, the energies and structures calculated with this functional compare very well to those obtained with the HSE functional. Inclusion of the Hartree-Fock exchange provides an accurate description of the band gap and the localized states that may be involved in charge trapping processes. The CP2K code uses a Gaussian basis set with an auxiliary plane-wave basis set [43]. Employing a Gaussian basis set has the advantage of allowing one to use fast analytical integration schemes, developed in quantum chemical methods, to calculate most of the Kohn-Sham matrix elements. The use of an auxiliary plane-wave basis set allows one to use fast Fourier transform algorithms for rapid convergence of the long-range Hartree terms. The Gaussian basis set employed for all atoms was a double-ζ basis set with polarization functions [44] in conjunction with the Goedecker-Teter-Hutter (GTH) pseudopotential [45]. Calculating hyperfine interactions necessitated the use of all electron basis sets using the Gaussian and augmented plane-wave (GAPW) approach. The basis sets with contraction schemes of (8831/831/1),(8411/411/11), and 6-311G** were used for silicon [46], oxygen [47], and Li [48], respectively. The plane-wave cutoff was set to 5440 eV (400 Ry).

To reduce the computational cost of nonlocal functional calculations, the auxiliary density matrix method (ADMM) was employed [49]. The density is mapped onto a much

sparser Gaussian basis set containing less diffuse and fewer primitive Gaussian functions than the one employed in the rest of the calculation. This allows the Hartree-Fock exchange terms, whose computational expense scales to the fourth power of the number of basis functions, to be calculated on a much smaller basis set than the rest of the calculation and therefore much faster.

All geometry optimizations were performed using the BFGS optimizer to minimize forces on atoms to within 37 pN (2.3 $\times 10^{-2}$ eV Å^{-1}). We modeled electron trapping in α-quartz cells containing 243 or 578 atoms. Most of the results reported below are for the cells containing 243 atoms, while the calculations performed in 578 atom cells were done to check for convergence in the studied properties. We have also checked the convergence in the 216-atom a-SiO_2 cells by comparing with the properties calculated in 648-atom cells. We have not included the results for the larger cells as they are consistent with those obtained in the smaller cells, indicating that the 216- and 243-atom cells of α quartz and a-SiO_2, respectively, are sufficient for this study. Barriers between configurations were calculated using the nudged elastic band method (NEB) [50,51]. Linear interpolation was used to generate 10 images to be optimized, with each of the images connected by a spring with a force constant of 19.5 eV Å^{-2}.

The calculated energies are corrected, where necessary, for the interaction between the charged defects using the method of Lany and Zunger [52,53]. This form of correction was chosen for its ability to describe the interactions of a localized charge and extended delocalized screening charge density, which comes out of charged DFT calculations [52]. The nature of the charge correction is the same for all the defects, irrespective of the character of localization. E_{corr} is calculated as

$$E_{\text{corr}} = \left[1 - \frac{\pi}{3\alpha}\left(1 - \frac{1}{\varepsilon}\right)\right]\frac{q^2\alpha}{2\varepsilon L}, \quad (1)$$

where ε is the macroscopic dielectric constant of SiO_2 (3.9 [54]), q is the charge of the cell (-1 in all cases), α is the Madelung constant for a single charge in a periodic array, and L is the supercell length. In this approach, E_{corr} for a single localized charge in a $3 \times 3 \times 3$ supercell of α quartz is constant and amounts to 0.18 eV. The charge corrections for the a-SiO_2 cells vary slightly according to the size of the cell and average at 0.17 eV. The difference in the charge corrections is due to the a-SiO_2 being less dense and the volume of the cell being larger than the α-quartz cells. We note that this correction term is only applied to localized states and not to the delocalized bandlike states.

To discuss the electron trapping by impurities in quartz and by perfect crystalline or amorphous SiO_2 structures, we compare the total energies of the initial and final states with the extra electron in the system, as illustrated in Fig. 1. The left diabatic curve (labeled as "initial state" in Fig. 1) represents the system with an extra electron in the initial state while the right curves (labeled as "final state 1 or 2") represent the final state with the electron localized on, for example, a Ge impurity or on a Si ion in the pure matrix after full geometry relaxation. E_B is the thermal barrier for electron trapping from the initial state to the localized state and E_T is the trapping energy, calculated as the total energy difference between the initial and final electronic states. In this work we discuss two different scenarios. Trapping from the initial state to the "final state 1" in Fig. 1 requires a thermal barrier to be overcome. The final state is higher in energy, corresponding to a negative trapping energy, and is thermodynamically less favorable than the initial electronic state. The second scenario corresponds to electron trapping from the initial state to the "final state 2" in Fig. 1. This electron trapping is barrier-less or has a small barrier; the final state is thermodynamically more favorable and corresponds to a positive E_T. The physical meaning of the initial and final states is discussed below for each particular system. We have also calculated optical excitation and ionization energies of trapped electrons using a self-consistent implementation of the maximum overlap method [55].

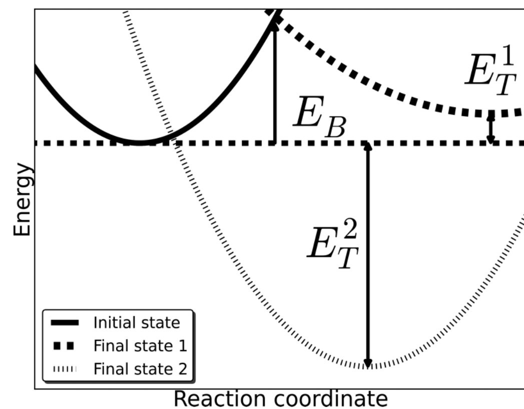

FIG. 1. A schematic of diabatic potential energy curves corresponding to an initial electronic state and two final electronic states of the system with extra electron. The energy labeled E_B is the thermal barrier to electron trapping. The energies labeled E_T are the trapping energies, calculated as the total energy difference between the initial and final state. There are two trapping energies shown in the figure. The physical meaning of the negative E_T^1 is that the final state is thermodynamically unstable with respect to the initial state. The final state 2 is thermodynamically stable with respect to the initial state.

III. RESULTS OF CALCULATIONS

A. Electron trapping in α quartz

To better appreciate the common features of extrinsic and intrinsic electron localization in α quartz and in amorphous silica, it is instructive to start from two known cases, where the extra electron localization is facilitated by impurities.

1. Ge-doped α quartz

The first case concerns the electron trapping by Ge impurities, substituting for Si, in both α quartz [14] and in a-SiO_2 [15]. The models of these centers have been recently reviewed by Griscom [16]. The cluster calculations by Pacchioni *et al.* of this so-called Ge electron center have demonstrated that a four-coordinated Ge atom in silica can trap an electron. This is accompanied by an orthorhombic distortion of the pseudotetrahedral Ge center, which results in two short and two long Ge–O bonds [56]. The periodic DFT calculations in a-SiO_2 structures by Du *et al.* have demonstrated that, in addition to the elongation of two Ge–O bonds, the O–Ge–O

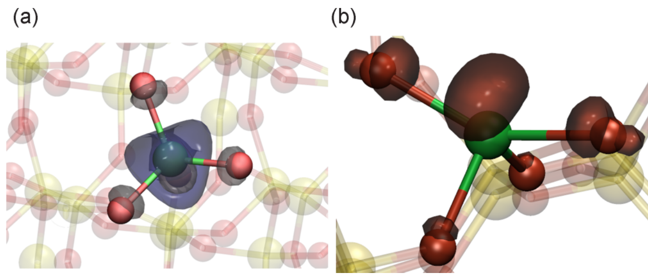

FIG. 2. (Color online) (a) The molecular orbital associated with the lowest unoccupied state in Ge-doped α quartz, strongly localized on the Ge impurity and its neighbors. (b) The spin density of the negatively charged Ge-doped α quartz with the spin density localized on the Ge center and its neighbors. The iso-value of the density surfaces is 0.02.

angle between the two elongated Ge–O bonds opens from about 110° to 170° to accommodate the extra electron [30]. This results from the repulsion between the localized electron and two neighboring oxygen ions.

The experimental characterization of electrons trapped in Ge-doped α quartz reveals two defects, the so-called Ge(I) and Ge(II) centers [14,57]. It has been suggested that these two defects reside on the same GeO_4 tetrahedron in both α quartz and a-SiO_2, with the Ge(I) center assigned as the ground state [14,16].

We performed calculations in 243 atom periodic cells of α quartz with one Si atom substituted for Ge. The geometry optimization in the neutral charge state maintains the tetrahedral coordination in pure bulk α quartz, however, the Ge–O bonds are slightly longer with two long (1.74 Å) Ge–O bonds, two short (1.73 Å) Ge–O bonds, and O–Ge–O angles of $\approx$109°. The calculated one-electron band gap of α quartz is 8.6 eV. The substitution of an Si atom for Ge induces an empty state at about 0.8 eV below the bottom of the conduction band, which is strongly localized on the Ge atom and its oxygen neighbors [see Fig. 2(a)].

An extra electron added to the cell is initially localized in this state ("initial state" in Fig. 1). The extra electron repels the two nearby oxygen atoms to lower the total energy by opening the O–Ge–O angle formed by the longer Ge–O bonds. This in turn localizes the electron further on the Ge atom and results in widening of the O–Ge–O angle. As a result, the two long Ge–O bonds elongate by 0.2 Å and become 1.9 Å and the O–Ge–O angle becomes 150°. The remaining two short Ge–O bonds extend slightly, up to 1.8 Å. The electron localization in this configuration is barrier-less, which corresponds to the transition from the initial state to the final state 2 in Fig. 1. We note that the bond lengths and angles of the Ge impurity center are asymmetric, both in the neutral and charged states. The spin density is strongly localized on the Ge atom and its oxygen neighbors [see Fig. 2(b)], with the Ge center possessing a Mulliken spin moment of 0.72. The electron trapping energy E_T in this state is 1.51 eV. Due to the localized nature of the initial state, this is effectively solely the relaxation energy of the system.

As mentioned above, it has been suggested that Ge(I) and Ge(II) electron spin resonance (ESR) signals can result from the electron trapping on a single GeO_4 tetrahedron [16]. We investigated whether an electron will localize in different configurations on the same GeO_4 tetrahedron by creating initial configurations that would favor these metastable states and then optimizing their geometry. In particular, we opened the five remaining O–Ge–O angles on this GeO_4 tetrahedron. This was accomplished by displacing two neighboring O ions of the original, ideal GeO_4 tetrahedron so that the two Ge–O bonds associated with the displaced O atoms are 1.9 Å and the angle between them is between 150° and 160°. After optimizing the geometry of the system in the negatively charged state, we found energy minima associated with all six combinations of Ge–O bond pairs, with the electron trapping energy E_T ranging between 1.36 and 1.51 eV across the six configurations. These results suggest that an electron can indeed localize on the Ge impurity in α quartz in different configurations.

All six configurations show qualitatively similar geometries, that is the elongation of two Ge–O bonds and the opening of O–Ge–O angle between them. However, there are quantitative differences in the extent of O–Ge–O angle opening which ranges from 132° to 150°. The electronic density of states of all six configurations shows an occupied one-electron level of between 4.18 and 4.39 eV below the bottom of the α-quartz conduction band, averaging at 4.31 eV. The relative energies of the six different configurations are plotted with respect to the O–Ge–O angle in Fig. 3. The general trend is that the lowest energy configuration has the widest O–Ge–O angle, and smaller O–Ge–O angles result in higher total energies. We believe that the smaller O–Ge–O angles are due to the asymmetric displacements induced by the Ge impurity in the neutral configuration and different local environments that each O–Ge–O angle exists in. This results in some of the O–Ge–O angles having larger space to relax into.

The calculated isotropic hyperfine constants on the Ge electron center range from −26.33 mT to −31.19 mT, with the lowest energy structure possessing an isotropic hyperfine constant of 29.17 mT. The calculated values are in the range of the experimental values of −28.47 mT and −28.96 mT reported by Isoya *et al.* for the Ge(I) and Ge(II) centers [14]. The barriers for transformations between the calculated configurations and their relation to Ge(I) and Ge(II) centers will be discussed in a separate publication.

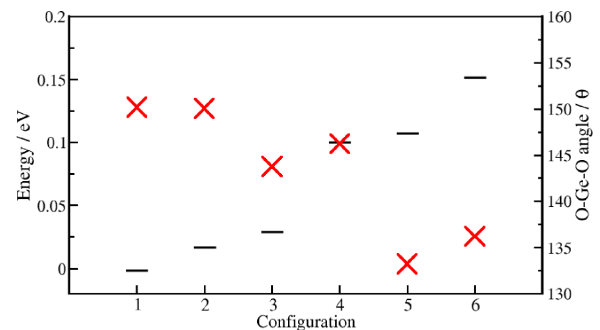

FIG. 3. (Color online) Energies of the six different electron trapping configurations in Ge-doped α quartz plotted alongside the O–Ge–O angle. The energies are shown on the left-hand side y axis and marked as black lines on the graph, while the O–Ge–O angles are shown on the right-hand side y axis and marked on the graph as red crosses.

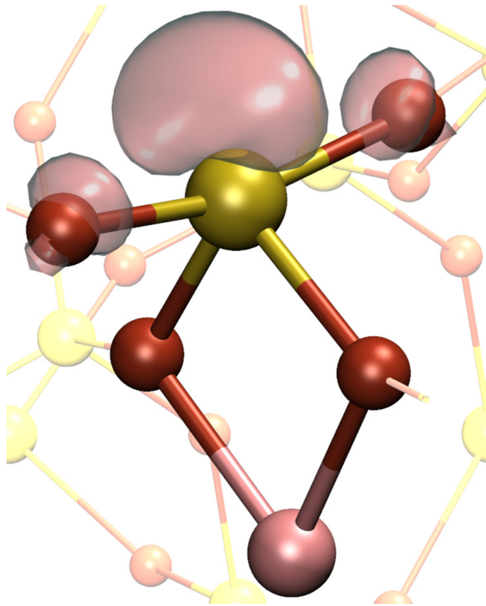

FIG. 4. (Color online) Atomic structure and spin density distribution of a Li center in α quartz. The Si atoms are the larger four-coordinated lighter spheres, O atoms are the smaller, darker two-coordinated spheres, and the Li ion is the large, light-colored sphere between two O atoms. The spin density is mainly localized on the Si atom in the center. The Li ion is bound to two bridging oxygens with an O-Li-O angle of 84°. The iso-value of spin density is equal to 0.015.

2. Li-doped α quartz

Jani *et al.* studied the effect of Li impurity in α quartz [17], particularly properties of $[AlO_4/Li]^0$ centers. A Li electron center in quartz was formed by a two-step irradiation process. The first irradiation step performed at 150–300 K moves the Li away from its Al counterpart [58]. The second step, performed after cooling the quartz sample down to 77 K, forms a $[SiO_4/Li]^0$ center. The ESR spectrum of this center shows a splitting of 0.09 mT from a ^{7}Li and 40.47 mT from a ^{29}Si. This center is stable below 180 K and has been characterized by Jani *et al.* as an extra electron trapped at a four-coordinated Si site with an adjacent Li^+ ion providing stability [17]. This model has been supported by early molecular cluster calculations by Wilson *et al.* [59], but no other calculations have been carried out to establish the structure of this center.

In our calculations, a Li atom was introduced into a $3 \times 3 \times 3$ supercell of α quartz and the geometry of the system was optimized in the neutral charge state. The Li atom occupies an interstitial position in the α-quartz lattice with a one-electron level $\approx$1.0 eV below the bottom of the α-quartz conduction band with no electron transfer taking place. We then investigated whether perturbing the lattice would induce electron transfer from the Li atom to Si ions. Opening an O–Si–O angle, in a manner similar to the O–Ge–O described above, and relaxing the structure results in the electron localization on the perturbed O–Si–O angle, as shown in Fig. 4. The relaxed structure has an extended O–Si–O angle of 150° while the Li ion is located 2.62 Å away from the Si center, bound to the two O neighbors, which are not associated with the O–Si–O angle opening. The spin density plot of the system in Fig. 4 shows that the unpaired spin is mostly localized on the Si atom (in the open O–Si–O angle) and its two oxygen neighbors. Mulliken population analysis reveals that the Li ion has charge of $+0.49\ |e|$ while the Si at the center of the wide O–Si–O angle has a Mulliken charge of $+1.1\ |e|$. The Mulliken charge of Si ions in quartz is $+1.43\ |e|$, indicating that the Si has gained electron density.

TABLE I. Hyperfine splittings and principle values of the hyperfine tensor (in mT) of the Li electron trap in α quartz. The experimental values of hyperfine interactions for the Li-doped quartz are shown for comparison.

Signal	Theor.	Expt. [17]
a_{iso} Si	43.07	40.47
a_{iso} Li	0.11	0.09
Principal values	0.089	0.088
	0.096	0.098
	0.16	0.15

The Li^+ ion is stabilized by the interaction with the lone pairs on the oxygen neighbors. The total energy of the Li stabilized electron center is 0.28 eV lower than that of the Li interstitial atom in α quartz, i.e., the trapping energy of the Li stabilized electron center is 0.28 eV. In this system, the initial state in terms of Fig. 1 corresponds to the electron localized on the Li atom and the final state is shown in Fig. 4. The small trapping energy reflects the fact that the initial state is already a deep electron trap. The barrier for transferring an electron from the atomic Li to the Si ion was calculated using the NEB method as 0.68 eV. De-trapping from this state requires overcoming a barrier of 0.96 eV. The occupied one-electron state of the unpaired electron is located 3.1 eV below the bottom of the quartz conduction band. This demonstrates the stabilizing role of the Li^+ ion in creating the $[SiO_4/Li]^0$ electron center. We note the similarity with electron trapping at low-coordinated Mg sites of the MgO (001) surface stabilized by a proton adsorbed on a neighboring O ion [60].

The calculated hyperfine splittings due to the interaction of the unpaired electron with the surrounding nuclei are shown in Table I and compared with the experimental results by Jani *et al.* [17]. The strongest hyperfine interaction is with the Si ion, with an isotropic hyperfine splitting of 43.07 mT. Smaller hyperfine splittings are on the Li ion and on O neighbors. The good agreement of the experimental and calculated ESR parameters gives confidence that our methods are capable of reliably describing the electron localization.

It is interesting to note that the experimentally measured ESR signal of the $[SiO_4/Li]^0$ center in Li-doped α quartz is reduced to zero at around 180 K [17]. Our calculated barrier for de-trapping is rather high at 0.96 eV, suggesting that it is perhaps not the electron transferring back to the Li atom which is responsible for the disappearance of the ESR signal. As mentioned earlier in this section, the interaction between the trapped electron and the Li ion provides a stabilizing Coulomb potential well for the trapped electron. As all the Si ions in α quartz are equivalent, diffusion of the Li ion into a nearby equivalent position provides an equally stabilizing Coulomb potential well for another equivalent Si atom. This

will lead to electron tunneling from the original Si site to a new site. This may offer a possible alternative explanation to the temperature dependence of the ESR signal. The calculated barrier for Li^+ ion diffusion in pure α quartz is 0.4 eV [61]. Using NEB we have calculated the barrier for diffusion of Li^+ of the $[SiO_4/Li]^0$ center between equivalent sites across a ring in α quartz as 0.56 eV. This Li^+ ion displacement is accompanied by an electron transfer to another Si site and is equivalent to diffusion of the whole center. At low temperatures the Li ions cannot overcome this diffusion barrier, hence the strong, discrete EPR signal. However, at increased temperatures Li ions start moving around and the ESR signal should decrease until it vanishes completely due to rapid electron transfer between equivalent Si sites.

To summarize, a common feature of both centers is that the electron localization on either the Ge or Si ion is accompanied by an energy gain, elongation of two metal-oxide bonds, and a significant opening of the –O–(Ge)Si–O– angle. This begs the question as to whether electron trapping in α quartz could also take place intrinsically, i.e., unaided by impurities. Previous calculations, in molecular cluster models with an α-quartz structure, indicate that electron trapping in α quartz does not occur spontaneously [56].

3. Pure bulk α quartz

When an extra electron is added in the perfect α-quartz structure and the geometry optimized using DFT, the electron stays fully delocalized at the bottom of the conduction band and there is no change in the lattice structure. We therefore investigated whether perturbations to the quartz structure could lead to trapping of an electron. The SiO_4 tetrahedra in α quartz are made up of two shorter Si–O bonds and two longer Si–O bonds. Displacing two O atoms around a Si atom associated with the two longer Si–O bonds so that an O–Si–O angle becomes greater than 135° and then optimizing the geometry leads to the extra electron localizing on the Si atom at the center of the tetrahedron. The O–Si–O angle associated with the two longer Si–O bonds was chosen by analogy with the lowest energy electron trap in Ge-doped α quartz. The geometry optimization further opens the O–Si–O angle to 161° and the two Si–O bonds elongate from 1.61 to 1.74 Å, while the other two bonds of the tetrahedron elongate to 1.69 Å. This structural relaxation is similar to the one observed for both Ge and Li electron centers.

However, the (self)-trapping energy of this system is −0.32 eV while the barrier to self-trapping an electron into this state from a delocalized conduction band state is 0.57 eV. This indicates that the self-trapped electron polaron state in pure α quartz is thermodynamically unstable with respect to the delocalized state (see Fig. 1). De-trapping from the localized state into the delocalized state requires overcoming a barrier of 0.25 eV. The O–Si–O angle at the maximum of this barrier is 134°. Mulliken population analysis reveals that the charge of the Si ion, on which the electron is localized, is $+1.04\ |e|$, significantly lower than the $+1.43\ |e|$ average charge of Si in α quartz. The localized electron creates a one-electron state 2.5 eV below the bottom of the α-quartz conduction band, which is principally Si and O "sp" in character. We note that the electron state of the Li electron center is lower by about 0.6 eV due to the Coulomb interaction with the nascent Li ion.

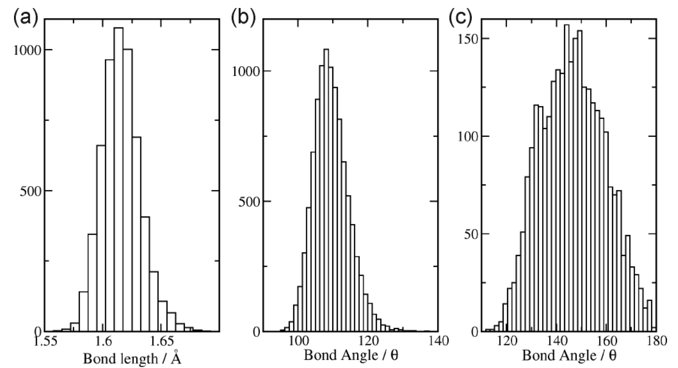

FIG. 5. Distributions of structural properties of a-SiO_2 optimized using DFT from 20 models of 216 atom periodic cells of a-SiO_2. (a) Shows a histogram of the Si–O bond lengths, (b) shows a histogram the O–Si–O bond angles, and (c) shows a histogram of the Si–O–Si bond angles.

B. Electron trapping in amorphous SiO_2

Electron trapping in a-SiO_2 was studied using 20 periodic models of bulk a-SiO_2 containing 216 atoms. The geometries of the ReaxFF generated amorphous structures were optimized in the neutral charge state within DFT and then an extra electron was added to each model. Figure 5 shows the distributions of Si–O bond lengths, and O–Si–O and Si–O–Si angles obtained after DFT geometry optimization of neutral cells. The geometrical properties of the optimized structures change slightly with respect to those obtained with ReaxFF. The Si–O bond lengths after DFT optimization average at 1.62 Å, ranging from 1.58 to 1.67 Å. The Si–O–Si angles average at 147°, ranging from 112° to 179°, while the O–Si–O angles average at 109°, ranging from 95° to 137°. The calculated total structure factors show three sharp peaks with averages at 1.61, 2.62, and 3.09 Å, in better agreement with experiment than the ReaxFF structures. Analysis of the ring size distribution after DFT optimization shows the four- and five-member rings to be dominant with smaller contributions from three- and six-member rings. The electronic structure calculations predict an average one-electron band gap of 8.1 eV, ranging from 7.7 to 8.3 eV over all 20 models. For comparison, the one-electron band gap of α quartz is 8.6 eV. The atomic coordinates of all 20 DFT optimized a-SiO_2 models are given in the Supplemental Material [62].

An extra electron initially occupies a state at the bottom of the a-SiO_2 conduction band. In all structures, this state is partially localized on several Si and O ions, as illustrated in Fig. 6 for one of the structures. The geometry of each of the systems was then optimized with the extra electron, resulting in barrier-less electron localization in four out of the 20 models. This localization was accompanied by a strong local distortion around a single SiO_4 tetrahedron, similar to the electron center relaxation in α quartz. In each of the four structures, the extra electron is localized on one Si ion, with the two O neighbors repelled so that an O–Si–O angle is opened to ≈172°, as shown in Fig. 7. The Si–O bonds making up

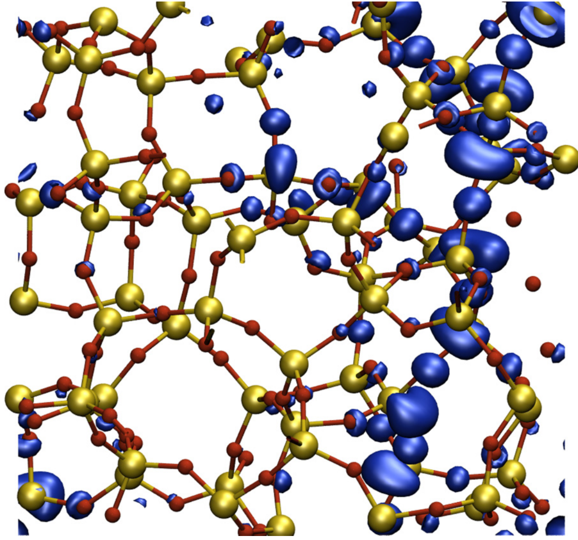

FIG. 6. (Color online) The square modulus of the wave function of an extra electron occupying the lowest state at the bottom of the conduction band of a-SiO_2. The bigger spheres connected to four atoms are Si atoms and the smaller spheres connected to two atoms are O atoms. The darker blobs represent the magnitude of the modulus of the wave function. The iso-value used to represent the square modulus of the wave function is 0.0005.

this O–Si–O angle elongate from 1.63 and 1.64 Å to 1.78 and 1.82 Å, respectively (see Fig. 7). The Mulliken population analysis shows that, as a result of the electron localization, the Si ion charge decreases by about 0.25 $|e|$. The average gain in energy resulting from the barrier-less electron localization E_T in the four models is 1.25 eV, ranging from 0.72 to 1.71 eV. The electron state occupied by the extra electron is located at $\approx 3.17 \pm 0.05$ eV below the bottom of the SiO_2 conduction band, indicating a deep electron trap.

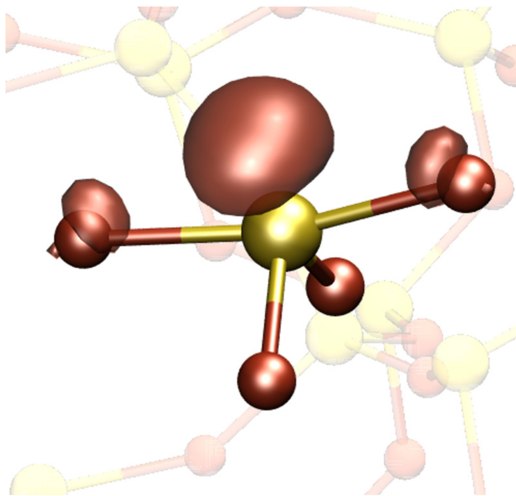

FIG. 7. (Color online) Atomic structure and spin density distribution of an intrinsic electron trap in a-SiO_2. We highlight the SiO_4 tetrahedron on which the electron traps and show the spin density only on the nearest ions. The spin density iso-value is 0.02.

TABLE II. Geometrical parameters and the average principal values of the hyperfine tensor the electron trap in a-SiO_2 from the four models. The bond lengths shown are with respect to the Si atom on which the electron is trapped.

Atom	Bond length (Å)	Values (mT)
Si		−50.98
		−45.45
		−45.23
O	1.82	−4.18
		−2.66
		−2.62
O	1.78	−5.71
		−4.36
		−4.30
O	1.70	−1.55
		−1.22
		−1.21
O	1.70	−1.58
		−1.26
		−1.26

The calculated values of the hyperfine splitting induced by the localized electron are shown in Table II. The strongest hyperfine interaction is with the Si ion; however, there is a significant interaction with the nearby oxygen atoms. Interestingly, some of the hyperfine interaction values are similar to those for the E′ center in amorphous silica. This is not surprising considering the strong electron localization on one Si ion. Although more models would be needed to give a more accurate distribution of the hyperfine values accessible to experiment, we believe these values are a good indication of where these hyperfine values may lie. We have also calculated the vertical ionization energies of this electron trap using the maximum overlap method [55]. They range from 2.99 to 3.35 eV. The nature of this transition is from the localized defect state to the lowest unoccupied state, which is also localized on the same Si ion. We note that the vertical ionization energy is very similar to the position of the one-electron defect level with respect to the bottom of the SiO_2 conduction band.

In all four cases we observe that the Si ion, on which the electron traps spontaneously, forms the widest O–Si–O angle in the sample, exceeding 132°. In the 16 remaining a-SiO_2 samples, where the distribution of O–Si–O angles was slightly narrower, the extra electron remained delocalized in static DFT calculations. To investigate this further, we introduced structural distortions to make two other random O–Si–O angles the widest in two separate systems. An angle in one of the systems was increased from 120.3° to 132.1°. Adding an extra electron into this system and optimizing the geometry results in the electron localizing on the Si ion within the changed angle and causes it to open further to 160.68°. An angle in a separate system was changed from 121.3° to 132.0°. When the electron was added to this system, the O–Si–O angle opened to 164.5°. These results demonstrate that, although a wide O–Si–O bond angle serves as an efficient precursor to electron trapping in amorphous silica, thermally activated trapping can also take place at other sites. These results also make apparent the link between the geometric structure of a trap and its electronic

properties and allow one to use the criterion of the wide O–Si–O angle as a *fingerprint* for identifying precursor sites for spontaneous electron localization in initial a-SiO_2 structure and estimating the concentration of such sites, as discussed below.

C. Concentration of electron trapping sites in a-SiO_2

As suggested above, by analyzing the structure of an a-SiO_2 sample for the presence of O–Si–O angles exceeding 132° one can estimate the lower limit of the concentration of precursor sites which can act as electron trapping centers. The results from the 20 models of a-SiO_2 samples indicate that the presence of an O–Si–O angle exceeding 132° always leads to spontaneous localization of extra electrons in a-SiO_2. This angle is at the tail of the O–Si–O angle distribution in regular SiO_2 structures constructed using the ReaxFF potential and optimized using DFT.

To test whether the existence of these precursor sites and their concentration depends on the model of amorphous structure and to obtain better statistics, we constructed three additional samples of amorphous SiO_2 using the BKS interatomic potentials [35], as described in Sec. II. These potentials are often used in studying the properties of a-SiO_2 and give structural parameters in good agreement with experimental data [37–39]. The three samples have dimensions of $50 \times 25 \times 5$ nm^3, $25 \times 12.5 \times 2.5$ nm^3, and $12.5 \times 7 \times 1.5$ nm^3 and include 401 760, 55 296, and 8 640 atoms, respectively. We searched these models for O–Si–O angles exceeding the fingerprint value of 132° to estimate the concentration of electron trapping precursor sites. The concentration of such sites in all models proved to be very similar and equal to $\approx 4 \times 10^{19}$cm^{-3}. It is interesting to note that, in spite of the difference in cell sizes and force fields used, this concentration agrees well with our original observation of four trapping sites in 20 216-atom samples. This agreement upon scaling demonstrates the universal character of the precursor site.

These results suggest that one could expect to find one or no trapped electron in the 648-atom periodic cell of a-SiO_2. To check that, we created two such models: one using the ReaxFF force field, and the other using BKS. The geometries of both models were then optimized within DFT using CP2K, as described above. These continuum random network models have perfect coordination of Si and O ions but different distributions of Si–O distances and O–Si–O angles and densities. Adding an extra electron in both models leads to its spontaneous localization on a widest O–Si–O angle, which is close to 132°. This further confirms our assertion that the predicted electron trapping in a-SiO_2 does not depend on the model of amorphous structure used.

IV. DISCUSSION AND CONCLUSIONS

Our calculations demonstrate the qualitatively similar character of extra electron localization in both crystalline and amorphous SiO_2. In α quartz, a substitutional Ge atom provides a local perturbation which facilitates the localization of an extra electron at the Ge site. A Li atom in α quartz donates an electron to a neighboring Si ion and further stabilizes the defect state by the Coulomb interaction between the trapped electron and the Li^+ ion. In both cases, the electron localization on Ge and Si ions is facilitated by the opening of the O–Si(Ge)–O angle. The electron localization in pure bulk α quartz requires opening the O–Si–O angle from 109° to 134°, but introducing this distortion costs 0.57 eV.

The distribution of geometrical parameters of a-SiO_2 leads to the existence of precursor Si sites, which can spontaneously trap an electron in a state $\approx$3.2 eV below the bottom of the conduction band. The estimated concentration of these precursor sites is $\approx 4 \times 10^{19}$ cm^{-3}. The large average distance between precursor sites suggests that diffusion of trapped electrons via a thermally activated tunneling mechanism should be quite inefficient and they are more likely to move via thermal activation into the mobility edge states of amorphous silica at high temperature.

Our results differ from those previously reported by Bersuker [18] and Camellone [19] which focused on the effect of the Si–O bond length and its relation to intrinsic electron trapping in SiO_2. Our results indicate that the O–Si–O angle is a more efficient precursor for electron trapping in SiO_2. The differences in our results from those presented by Camellone *et al.* could stem from our use of a nonlocal functional as opposed to the generalized gradient approximation [19] as GGA tends to underestimate the degree of electron or hole localization [63,64].

Predicting the electron and hole trapping in insulators is challenging due to the well-known self-interaction error inherent in local functionals used in most DFT calculations [65]. In this work we used the nonlocal functional PBE0_TC_LRC and obtained the electron localization in Ge and Li electron centers in α quartz and in pure bulk α quartz and a-SiO_2. The hyperfine splitting parameters calculated for both Ge and Li centers in α quartz are in good agreement with the experimental values, suggesting that PBE0_TC_LRC can describe the electronic structure of electron traps in silica relatively accurately.

The high volume concentration of the large O–Si–O angle electron trapping precursor sites suggests that the electron trapping can be abundant in a-SiO_2 samples. However, identifying these electron traps in relatively pure bulk samples may require irradiating at liquid nitrogen temperatures, where both trapped electrons and holes are immobile [3]. Our results suggest that trapped electrons can be stable even at room temperature. However, trapped holes become mobile below 200 K and can recombine with electrons. Our results also support the common perception that the abundance of impurities, such as Al, Ge, Li, Na, and water in quartz as well as in silica glass samples may lead to efficient electron trapping by impurity centers and further hamper the identification of electron traps in a pure silica network.

We correlate these states to electron traps identified experimentally in MOS devices [66] at an energy of 2.8 eV below the conduction band of a-SiO_2 grown on Si and SiC crystals [21–24]. These traps were populated by illuminating the MOS structures by photons of energy sufficient to excite electrons from the semiconductor valence or conduction band above the edge of the SiO_2 conduction band. These electron traps have initially been correlated with oxygen deficient centers at the near-interfacial oxide [22,23,29]. However, later experiments on nitridated SiC/SiO_2 samples questioned this attribution, particularly when taking into account the fact that

the density of known O-deficiency centers (E'_γ and E'_δ centers) rarely approaches the density range of $10^{13}cm^{-2}$ found for the 2.8-eV deep electron traps. Although these electron traps are especially pronounced in 4H-SiC/SiO_2 devices, they seem to play a role in all devices containing SiO_2 as the insulating material, suggesting that they may be intrinsic to the oxide. For instance, these traps are expected to appear below the conduction band of Si nanocrystals in the case of quantum confinement [67,68].

We suggest that the intrinsic electron traps in a-SiO_2 discussed in this work could be good candidates for understanding these data. The calculated concentration of the electron traps approaches the experimentally observed value for the states filled by photo-stimulated tunneling from the SiO_2 valence band. However, populating such a density of electron traps via electron injection from an electrode through the SiO_2 conduction band should be much less efficient because an electron capture event requires dissipating about 1.5 eV of relaxation energy into phonons during the trapping process. This process is likely to be slower than fast electron transport in the conduction band of thin oxide towards an opposite electrode. In order to keep the additional (unpaired) electrons on these centers one must ensure sufficiently high strength of electric field externally applied to the interface. The latter can hardly be realized under the conditions of an ESR experiment because the presence of conducting electrodes impairs the quality factor of the microwave resonator. Furthermore, all available experimental evidence concerns interfaces of SiO_2 with semiconducting materials (Si, SiC), which might suggest that the experimentally observed high probability of electron trap occupation may be related to the strain in the SiO_2 network near the interface, while in the bulk of the film their concentration may be lower. The observed trap photoionization energy at 2.8 eV is between the values calculated for α quartz (2.5 eV) and a-SiO_2 (3.0 eV). Our results indicate that the geometry of the oxide structure can significantly affect the position of the defect level, and the discrepancy between the experimental value and our a-SiO_2 value may reflect the higher oxide density in thermally grown oxides [69,70] rather than the density obtained in this work.

To summarize, our results demonstrate that, similar to holes [3], electrons can be trapped at structural precursor sites in an amorphous silica matrix, forming deep electron states in the oxide band gap. The geometric structure of trapped electron centers in a-SiO_2 are qualitatively similar to the intrinsic and extrinsic electron trapping centers in α quartz. In a-SiO_2, these states may be responsible for the electron trapping observed at interfaces of SiO_2-based MOS devices and should be present in bulk SiO_2 samples.

ACKNOWLEDGMENTS

The authors acknowledge EPSRC and the EU FP7 project MORDRED (EU Project Grant No. 261868) and COST Action CM1104 for financial support. We are grateful to K. Tanimura, A. Kimmel, M. Wolf, G. Bersuker, A. Stesmans, T. Grasser, B. Kaczer, and F. Schanovsky for useful and stimulating discussions. We are also grateful to S. Agnello and S. Bradley for their comments on the manuscript. We would like to thank the UK's HPC Materials Chemistry Consortium, which is funded by EPSRC (EP/F067496), for providing computer resources on the UK's national high-performance computing service HECToR and Archer.

[1] D. M. Fleetwood, S. T. Pantelides, and R. D. Schrimpf (eds.), *Defects in Microelecronic Materials and Devices* (CRC Press, Boca Raton, 2009).
[2] T. Y. Chan, K. K. Young, and C. Hu, IEEE Elect. Dev. Lett. **8**, 93 (1987).
[3] D. L. Griscom, J. Non-Cryst. Solids **352**, 2601 (2006).
[4] G. Pacchioni and A. Basile, Phys. Rev. B **60**, 9990 (1999).
[5] A. V. Kimmel, P. V. Sushko, and A. L. Shluger, J. Non-Cryst. Solids **353**, 599 (2007).
[6] S. Sicolo, G. Palma, C. Di Valentin, and G. Pacchioni, Phys. Rev. B **76**, 075121 (2007).
[7] L. Skuja, J. Non-Cryst. Solids **239**, 16 (1998).
[8] G. Pacchioni, L. Skuja, and D. L. Griscom (eds.), *Defects in SiO_2 and Related Dielectrics: Science and Technology* (Nato Science Series, Springer, New York, 2000).
[9] D. L. Griscom, Physics Research International **2013**, 379041 (2013).
[10] E. H. Nicollian, C. N. Berglund, P. F. Schmidt, and J. M. Andrews, J. Appl. Phys. **42**, 5654 (1971).
[11] A. Hartstein and D. R. Young, Appl. Phys. Lett. **38**, 631 (1981).
[12] V. V. Afanas'ev, J. M. M. de Nijs, P. Balk, and A. Stesmans, J. Appl. Phys. **78**, 6481 (1995).
[13] V. V. Afanas'ev and A. Stesmans, Appl. Phys. Lett. **71**, 3844 (1997).
[14] J. Isoya, J. A. Weil, and R. F. C. Claridge, J. Chem. Phys. **69**, 4876 (1978).
[15] D. L. Griscom, J. Non-Cryst. Solids **357**, 1945 (2011).
[16] D. L. Griscom, Opt. Mater. Express **1**, 400 (2011).
[17] M. G. Jani, L. E. Halliburton, and A. Halperin, Phys. Rev. Lett. **56**, 1392 (1986).
[18] G. Bersuker, A. Korkin, Y. Jeon, and H. Huff, Appl. Phys. Lett. **80**, 832 (2002).
[19] M. Farnesi Camellone, J. C. Reiner, U. Sennhauser, and L. Schlapbach, Phys. Rev. B **76**, 125205 (2007).
[20] L. Giordano, P. V. Sushko, G. Pacchioni, and A. L. Shluger, Phys. Rev. Lett. **99**, 136801 (2007).
[21] V. V. Afanas'ev and A. Stesmans, Phys. Rev. Lett. **78**, 2437 (1997).
[22] V. V. Afanas'ev and A. Stesmans, Appl. Phys. Lett. **70**, 1260 (1997).
[23] V. V. Afanas'ev and A. Stesmans, Microelectron. Eng. **36**, 149 (1997).
[24] V. V. Afanas'ev and A. Stesmans, J. Phys.: Condens. Matter **9**, L55 (1997).

[25] V. V. Afanas'ev, A. Stesmans, M. Bassler, G. Pensl, and M. J. Schulz, Appl. Phys. Lett. **76**, 336 (2000).
[26] N. S. Saks and A. K. Agarwal, Appl. Phys. Lett. **77**, 3281 (2000).
[27] N. S. Saks, S. S. Mani, and A. K. Agarwal, Appl. Phys. Lett. **76**, 2250 (2000).
[28] V. V. Afanas'ev, A. Stesmans, F. Ciobanu, G. Pensl, K. Y. Cheong, and S. Dimitrijev, Appl. Phys. Lett. **82**, 568 (2003).
[29] V. V. Afanas'ev, F. Ciobanu, S. Dimitrijev, G. Pensl, and A. Stesmans, J. Phys.: Condens. Matt. **16**, S1839 (2004).
[30] J. Du, L. R. Corrales, K. Tsemekhman, and E. J. Bylaska, Nucl. Instrum. Meth. B **255**, 188 (2007).
[31] A. M. El-Sayed, M. B. Watkins, A. L. Shluger, and V. V. Afanas'ev, Microelectron. Engineering **109**, 68 (2013).
[32] A. C. T. van Duin, A. Strachan, S. Stewman, Q. Zhang, X. Xu, and W. Goddard, J. Phys. Chem. A **107**, 3803 (2003).
[33] J. C. Fogarty, H. M. Aktulga, A. Y. Grama, A. C. T. van Duin, and S. A. Pandit, J. Chem. Phys. **132**, 174704 (2010).
[34] R. T. Sanderson, *Chemical Bonds and Bond Energy* (Academic Press, Waltham, 1976).
[35] B. W. H. van Beest, G. J. Kramer, and R. A. van Santen, Phys. Rev. Lett. **64**, 1955 (1990).
[36] S. Plimpton, J. Comp. Phys. **117**, 1 (1995).
[37] S. Mukhopadhyay, P. V. Sushko, A. M. Stoneham, and A. L. Shluger, Phys. Rev. B **70**, 195203 (2004).
[38] A. Roder, W. Kob, and K. Binder, J. Chem. Phys. **114**, 7602 (2001).
[39] K. Vollmayr, W. Kob, and K. Binder, Phys. Rev. B **54**, 15808 (1996).
[40] J. VandeVondele, M. Krack, F. Mohamed, M. Parrinelo, T. Chassaing, and J. Hutter, Comp. Phys. Comm. **167**, 103 (2005).
[41] M. Guidon, J. Hutter, and J. VandeVondele, J. Chem. Theory Comput. **5**, 3013 (2009).
[42] J. Heyd, G. E. Scuseria, and M. Ernzerhof, J. Chem. Phys. **124**, 219906 (2006).
[43] G. Lippert, J. Hutter, and M. Parrinello, Mol. Phys. **92**, 477 (1997).
[44] J. VandeVondele and J. Hutter, J. Chem. Phys. **127**, 114105 (2007).
[45] S. Goedecker, M. Teter, and J. Hutter, Phys. Rev. B **54**, 1703 (1996).
[46] B. Civalleri and P. Ugliengo, J. Phys. Chem. B **104**, 519 (2000).
[47] M. D. Towler, N. L. Allan, N. M. Harrison, V. R. Saunders, W. C. Mackrodt, and E. Apra, Phys. Rev. B **50**, 5041 (1994).
[48] R. Krishnan, J. S. Binkley, R. Seeger, and J. A. Pople, J. Chem. Phys. **72**, 650 (1980).
[49] M. Guidon, J. Hutter, and J. VandeVondele, J. Chem. Theory Comput. **8**, 2348 (2010).
[50] G. Henkelman, B. P. Uberuaga, and H. Jónsson, J. Chem. Phys. **113**, 9901 (2000).
[51] R. Elber and M. Karplus, Chem. Phys. Lett. **139**, 375 (1987).
[52] S. Lany and A. Zunger, Modelling Simul. Mater. Sci. Eng. **17**, 084002 (2009).
[53] H.-P. Komsa, T. T. Rantala, and A. Pasquarello, Phys. Rev. B **86**, 045112 (2012).
[54] S. Muller and T. I. Kamins, *Device Electronics for Integrated Circuits* (Wiley, New York, 2003).
[55] A. T. B. Gilbert, N. A. Besley, and P. M. W. Gill, J. Phys. Chem. A **112**, 13164 (2008).
[56] G. Pacchioni and C. Mazzeo, Phys. Rev. B **62**, 5452 (2000).
[57] W. Hayes and T. J. L. Jenkin, J. Phys. C: Solid State Phys. **19**, 6211 (1986).
[58] M. E. Markes and L. E. Halliburton, J. Appl. Phys. **50**, 8172 (1979).
[59] T. M. Wilson, J. A. Weil, and P. S. Rao, Phys. Rev. B **34**, 6053 (1986).
[60] D. Ricci, C. Di Valentin, G. Pacchioni, P. V. Sushko, A. L. Shluger, and E. Giamello, J. Amer. Chem. Soc. **125**, 738 (2003).
[61] A. Sartbaeva, S. A. Wells, and S. A. T. Redfern, J. Phys.: Condens. Matter **16**, 8173 (2004).
[62] See Supplemental Material at http://link.aps.org/supplemental/10.1103/PhysRevB.89.125201 for XYZ coordinates of a-SiO_2 structures studied throughout text.
[63] M. Städele, M. Moukara, J. A. Majewski, P. Vogl, and A. Gorling, Phys. Rev. B **59**, 10031 (1999).
[64] A. D. Becke, J. Chem. Phys. C **98**, 5648 (1993).
[65] J. L. Gavartin, P. V. Sushko, and A. L. Shluger, Phys. Rev. B **67**, 035108 (2003).
[66] I. Pintilie, C. M. Teodorescu, F. Moscatelli, R. Nipoti, A. Poggi, S. Solmi, L. S. L. vlie, and B. G. Svensson, J. Appl. Phys. **108**, 024503 (2010).
[67] V. V. Afanas'ev and A. Stesmans, Phys. Rev. B **59**, 2025 (1999).
[68] G. Seguini, S. Schamm-Chardon, P. Pellegrino, and M. Perego, Appl. Phys. Lett. **99**, 082107 (2011).
[69] A. C. Diebold, D. Venables, Y. Chabal, D. Muller, M. Weldon, and E. Garfunkel, Mater. Sci. Semicond. Process. **2**, 103 (1999).
[70] A. Waseda and K. Fujii, IEEE Trans. Instrum. Meas. **56**, 628 (2007).